

A nonlinear dynamic corotational finite element model for submerged pipes

F H de Vries^{1*}, H J M Geijselaers¹, A H van den Boogaard¹ and A Huisman²

¹University of Twente, Faculty of Engineering Technology, P.O. Box 217, 7500 AE Enschede, The Netherlands

²Allseas Engineering B.V., Delft, The Netherlands

*Corresponding author: f.h.devries@utwente.nl

Abstract. A three dimensional finite element model is built to compute the motions of a pipe that is being laid on the seabed. This process is geometrically nonlinear, therefore co-rotational beam elements are used. The pipe is subject to static and dynamic forces. Static forces are due to gravity, current and buoyancy. The dynamic forces exerted by the water are incorporated using Morison's equation. The dynamic motions are computed using implicit time integration. For this the Hilber-Hughes-Taylor method is selected. The Newton-Raphson iteration scheme is used to solve the equations in every time step. During laying, the pipe is connected to the pipe laying vessel, which is subject to wave motion. Response amplitude operators are used to determine the motions of the ship and thus the motions of the top end of the pipe.

1. Introduction

Typical numerical simulations of offshore pipelaying tend to have high computational costs. This is due to the long time period of a simulation in combination with several variables, such as wave direction and water depth. Commercial software is available for these type of simulations, such as Offpipe [1], PipeLay [2] and Orcaflex [3]. Each of these software packages has its possibilities as well as limitations. Due to increased analysis demands and market trends there is a need for quicker and more efficient software. The current work brings existing methods together in order to build an efficient dynamic model for pipe laying simulations.

Offshore pipelay analyses are typically performed using a Finite Element approach. In these analyses large rotations of the elements occur. In literature several methods for large rotations can be found. Reissner [4] and Simo and Vu Quoc [5], [6] developed the geometrically exact beam method. This method is named exact because no assumptions have been made on the size of the deformations. However, since discretization will be used, this method is still an approximation. This method converges in a small number of iterations for small beam lengths. However, to analyze offshore pipe laying efficiently, long elements are required. The geometrically exact method requires a large number of iterations to converge when using long elements.

An alternative method for large rotations is the absolute nodal coordinate formulation, presented by Shabana [7]. An advantage of this method is that it results in a constant mass matrix. However when using a time integration method from the Newmark-family [8], the mass matrix is not inverted in every iteration. Thus the only advantage of a constant mass matrix is that it does not need to be rotated. Disadvantages of this method are the more complex stiffness matrix and the larger number of degrees



of freedom compared to the co-rotational method. Furthermore Romero [9] and Bauchau and Han [10] compared the absolute nodal coordinate and geometrically exact formulations. In both papers, no improvements of accuracy or computational costs are found for the absolute nodal coordinate formulation.

Shabana [11] suggested a substructuring technique with a floating frame of reference. The deformations of the substructures are described by elastic vibration modes. This method is often used in multibody dynamics. Disveld [12] investigated in his MSc thesis if this method would be more efficient for offshore pipelaying application. Additionally, he investigated a recursive method with two fixed ends. These methods were shown to be less efficient compared to the co-rotational finite element method.

The chosen method for large rotations in the current numerical model is therefore the co-rotational method, presented in Section 2. The co-rotational method has been well established in literature [13], [14] and more recently [15], [16]. The formulation used in the current model is the method of Crisfield [17][18].

General distributed loads are added in the global coordinate system in Section 3. Thereafter two special kinds of distributed loads are considered. In Section 4 buoyancy is added using the method of Yazdchi [19]. New in this paper is the addition of equivalent moments for the buoyancy due to a distributed pressure. Furthermore, when the pipe moves through the water, forces are exerted by the water on the pipe. These hydrodynamic forces are included in the model using Morison's equation [20]. This also accounts for the forces due to the velocity and acceleration of the water, as can be seen in Section 5.

To be able to use large time steps in the numerical time integration, implicit time integration is chosen. A well-known method is the Newmark- β method [8], which requires parameters β and γ . If these parameters are chosen at $\beta = 1/4$ and $\gamma = 1/2$, the method is second order accurate and unconditionally stable for linear systems. However the current model is nonlinear. To maintain stability numerical damping can be added by increasing parameter γ , but then the second order accuracy is lost. For this reason, for the Hilber-Hughes-Taylor method, or HHT- α method [21], is selected, which is an expansion of the Newmark- β method. The HHT- α method uses a parameter α to include damping and is second order accurate independent of its parameter. Further details of this method can be found in [21]. In Section 6 both static and dynamic examples using the presented method are presented.

2. Three dimensional co-rotational method

This section is an introduction to the co-rotational beam element in a three dimensional space. This element has two nodes. Each node has six degrees of freedom, three translations and three rotations. The foundation of the method is that it uses a local coordinate system to calculate small strains. This is presented in Section 2.1. This local coordinate system is rotated to the global coordinate system. The corresponding rotation matrix is shown in Section 2.2.

Because the co-rotational method is geometrically nonlinear, an iterative solution procedure is needed. The Newton-Raphson method is selected.

$$\mathbf{u}_{sys}^{n+1} = \mathbf{u}_{sys}^n - K_{sys}^{-1} \mathbf{F}_{sys} \quad (1)$$

Here \mathbf{F}_{sys} is the system force vector. This vector is built using the global force vector and the external force vector: $\mathbf{F} = \mathbf{F}_{int} - \mathbf{F}_{ext}$. The internal force vector is derived in section 2.3. K_{sys} is the system stiffness matrix. This matrix is assembled from the tangent stiffness matrices of all elements. The tangent stiffness matrix is presented in section 2.4.

2.1. Local coordinate system

In a co-rotational formulation a local 'co-rotational' coordinate frame is introduced. The origin of this frame is placed on the first node of the element. The local coordinate frame is placed such that the x-axis runs through the first and the second node. In other words the displacements in local y- and z-

direction are always zero at the nodes. This placement of the coordinate system results in only seven local degrees of freedom.

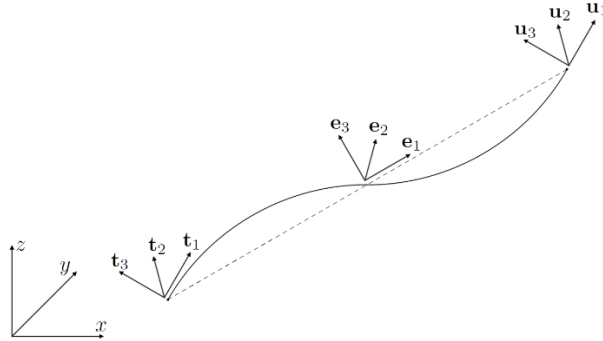


Figure 1. Co-rotational beam element with orthogonal unit vectors to define rotations

$$\mathbf{p}_l = [\psi_1, \theta_1, \phi_1, u, \psi_2, \theta_2, \phi_2]^T \quad (2)$$

An important factor when rotating in three dimensions is that the rotations are in general not commutative. This means that a rotation cannot be added to another rotation. The three dimensional rotations are implemented using nodal triads. Detailed derivations can be found in [18]. For each element, two nodal triads, T and U, and one element triad, E, are defined. This can be seen in Figure 1. Each triad contains three orthogonal unit vectors. The unit vectors of the three triads are named \mathbf{t}_i , \mathbf{e}_i and \mathbf{u}_i .

$$\mathbf{T} = [\mathbf{t}_1, \mathbf{t}_2, \mathbf{t}_3] \quad \mathbf{E} = [\mathbf{e}_1, \mathbf{e}_2, \mathbf{e}_3] \quad \mathbf{U} = [\mathbf{u}_1, \mathbf{u}_2, \mathbf{u}_3] \quad (3)$$

These unit vectors define the local rotations of the element nodes. The middle triad defines the element coordinate system. As shown by Crisfield [18], these unit vectors can be used to find the local rotations.

$$\begin{aligned} 2 \sin \psi_1 &= -\mathbf{t}_3^T \mathbf{e}_2 + \mathbf{e}_3^T \mathbf{t}_2 \\ 2 \sin \theta_1 &= \mathbf{t}_3^T \mathbf{e}_1 - \mathbf{e}_3^T \mathbf{t}_1 \\ 2 \sin \phi_1 &= -\mathbf{t}_2^T \mathbf{e}_1 + \mathbf{e}_2^T \mathbf{t}_1 \\ 2 \sin \psi_2 &= -\mathbf{u}_3^T \mathbf{e}_2 + \mathbf{e}_3^T \mathbf{u}_2 \\ 2 \sin \theta_2 &= \mathbf{u}_3^T \mathbf{e}_1 - \mathbf{e}_3^T \mathbf{u}_1 \\ 2 \sin \phi_2 &= -\mathbf{u}_2^T \mathbf{e}_1 + \mathbf{e}_2^T \mathbf{u}_1 \end{aligned} \quad (4)$$

After each iteration, nodal triads T and U are updated as follows.

$$\begin{aligned} \mathbf{T}_{n+1} &= \Delta \mathbf{T}(\Delta \boldsymbol{\alpha}) \mathbf{T}_n \\ \mathbf{U}_{n+1} &= \Delta \mathbf{U}(\Delta \boldsymbol{\beta}) \mathbf{U}_n \end{aligned} \quad (5)$$

Here $\Delta \boldsymbol{\alpha}$ and $\Delta \boldsymbol{\beta}$ are the iterative spin variables. These variables are the update increments of the angles at the end of an iteration. They are non-additive and represent the vector about which the nodal system is rotated. The length of the vector is the angle. $\Delta \mathbf{T}$ and $\Delta \mathbf{U}$ are rotation matrices. Here it is chosen to use Rodrigues rotation matrix [22].

The element triad E is updated differently. For this matrix first a rotation matrix from the first node to the second node is determined.

$$\Delta \mathbf{R}(\boldsymbol{\gamma}) = \mathbf{U} \mathbf{T}^T \quad (6)$$

Spurrier's algorithm [23] is applied to $\Delta \mathbf{R}$ to find spin variable $\boldsymbol{\gamma}$. This is used to find the mean rotation $\bar{\mathbf{R}}$.

$$\bar{\mathbf{R}} = \Delta \mathbf{R}_m \left(\frac{\mathbf{Y}}{2} \right)^T \quad (7)$$

Here $\Delta \mathbf{R}_m(\mathbf{Y}/2)$ is obtained using the Rodrigues rotation matrix. The mean rotation $\bar{\mathbf{R}}$ is used to find the matrix E. First the vector \mathbf{e}_1 is obtained by

$$\mathbf{e}_1 = \frac{1}{L} (\mathbf{x}_{21} + \mathbf{d}_{21}) = \frac{1}{L} \begin{bmatrix} x_2 - x_1 + u_2 - u_1 \\ y_2 - y_1 + v_2 - v_1 \\ z_2 - z_1 + w_2 - w_1 \end{bmatrix} \quad (8)$$

Here x_i, y_i and z_i are the coordinates of node i and u_i, v_i and w_i are the displacements of node i . These are all in the global coordinate system. Using Crisfield's mid-point rule approximation and $\bar{\mathbf{R}} = [\mathbf{r}_1, \mathbf{r}_2, \mathbf{r}_3]$, \mathbf{e}_2 and \mathbf{e}_3 are found.

2.2. Rotation matrix

A rotation matrix is derived to rotate from the local coordinate system to the global coordinate system. This is done by taking the variation of the local variables.

$$\delta \mathbf{p}_l = [\delta \psi_1, \delta \theta_1, \delta \phi_1, \delta u, \delta \psi_2, \delta \theta_2, \delta \phi_2]^T = \mathbf{B} \delta \mathbf{p} \quad (9)$$

This derivation can be found in [18]. Note that a different coordinate system is used here. The resulting rotation matrix is

$$\mathbf{B} = \begin{bmatrix} \frac{1}{2 \cos \psi_1} (\mathbf{t}_2^T \mathbf{Q}(\mathbf{r}_3) - \mathbf{t}_3^T \mathbf{Q}(\mathbf{r}_2) + [\mathbf{0}, \mathbf{e}_2^T \tilde{\mathbf{t}}_3 - \mathbf{e}_3^T S \tilde{\mathbf{t}}_2, \mathbf{0}, \mathbf{0}]) \\ \frac{-1}{2 \cos \theta_1} (\mathbf{t}_1^T \mathbf{Q}(\mathbf{r}_3) + [\mathbf{t}_3^T \mathbf{A}, \mathbf{e}_1^T \tilde{\mathbf{t}}_3 - \mathbf{e}_3^T \tilde{\mathbf{t}}_1, -\mathbf{t}_3^T \mathbf{A}, \mathbf{0}]) \\ \frac{1}{2 \cos \phi_1} (\mathbf{t}_1^T \mathbf{Q}(\mathbf{r}_2) + [\mathbf{t}_2^T \mathbf{A}, \mathbf{e}_1^T \tilde{\mathbf{t}}_2 - \mathbf{e}_2^T \tilde{\mathbf{t}}_1, -\mathbf{t}_2^T \mathbf{A}, \mathbf{0}]) \\ [-\mathbf{e}_1^T, \mathbf{0}, \mathbf{e}_1^T, \mathbf{0}] \\ \frac{1}{2 \cos \psi_2} (\mathbf{u}_2^T \mathbf{Q}(\mathbf{r}_3) - \mathbf{u}_3^T \mathbf{Q}(\mathbf{r}_2) + [\mathbf{0}, \mathbf{0}, \mathbf{0}, \mathbf{e}_2^T \tilde{\mathbf{u}}_3 - \mathbf{e}_3^T \tilde{\mathbf{u}}_2]) \\ \frac{-1}{2 \cos \theta_2} (\mathbf{u}_1^T \mathbf{Q}(\mathbf{r}_3) + [\mathbf{u}_3^T \mathbf{A}, \mathbf{0}, -\mathbf{u}_3^T \mathbf{A}, \mathbf{e}_1^T \tilde{\mathbf{u}}_3 - \mathbf{e}_3^T \tilde{\mathbf{u}}_1]) \\ \frac{1}{2 \cos \phi_2} (\mathbf{u}_1^T \mathbf{Q}(\mathbf{r}_2) + [\mathbf{u}_2^T \mathbf{A}, \mathbf{0}, -\mathbf{u}_2^T \mathbf{A}, \mathbf{e}_1^T \tilde{\mathbf{u}}_2 - \mathbf{e}_2^T \tilde{\mathbf{u}}_1]) \end{bmatrix} \quad (10)$$

This is a 7x12 matrix. Here $\tilde{\mathbf{t}}_i$ is the skew symmetric cross product matrix of vector \mathbf{t}_i . Furthermore Q is the following 3x12 matrix.

$$\mathbf{Q}(\mathbf{r}_i) = [-Q_1(\mathbf{r}_i), Q_2(\mathbf{r}_i), Q_1(\mathbf{r}_i), Q_2(\mathbf{r}_i)] \quad (11)$$

with

$$\begin{aligned} Q_1(\mathbf{r}_i) &= -\frac{1}{2} \mathbf{r}_i^T \mathbf{e}_1 \mathbf{A} - \frac{1}{2} (\mathbf{e}_1 + \mathbf{r}_1) \mathbf{r}_i^T \mathbf{A} \\ Q_2(\mathbf{r}_i) &= -\frac{1}{2} \tilde{\mathbf{r}}_i + \frac{1}{4} \mathbf{r}_i^T \mathbf{e}_1 \tilde{\mathbf{r}}_i + \frac{1}{4} (\mathbf{e}_1 + \mathbf{r}_1) \mathbf{e}_1^T \tilde{\mathbf{r}}_i \end{aligned} \quad (12)$$

and

$$\mathbf{A} = \frac{1}{L} (\mathbf{I} - \mathbf{e}_1^T \mathbf{e}_1). \quad (13)$$

Here I is a 3x3 identity matrix.

2.3. Internal forces

The three dimensional stiffness matrix can be found in many textbooks like [24]. It is presented as a 12x12 matrix. However the size of this matrix can be reduced when using the co-rotational method. Since the number of local degrees of freedom is reduced to seven, the local stiffness matrix is reduced to 7x7.

$$K_l = \frac{1}{L_0} \begin{bmatrix} GJ & 0 & 0 & 0 & -GJ & 0 & 0 \\ 0 & 4EI & 0 & 0 & 0 & 2EI & 0 \\ 0 & 0 & 4EI & 0 & 0 & 0 & 2EI \\ 0 & 0 & 0 & EA & 0 & 0 & 0 \\ -GJ & 0 & 0 & 0 & GJ & 0 & 0 \\ 0 & 2EI & 0 & 0 & 0 & 4EI & 0 \\ 0 & 0 & 2EI & 0 & 0 & 0 & 4EI \end{bmatrix} \quad (14)$$

The stiffness matrix multiplied by the local displacements vector yields the local element forces.

$$\mathbf{f}_l = K_l \mathbf{p}_l \quad (15)$$

The forces in the global coordinate system are found by rotating the local forces.

$$\mathbf{F}_{int} = \mathbf{B}^T \mathbf{f}_l \quad (16)$$

2.4. Consistent tangent stiffness

The tangential stiffness matrix is found by taking the variation of the forces in the global coordinate system.

$$\begin{aligned} \delta \mathbf{F}_{int} &= \mathbf{K} \delta \mathbf{p} = \mathbf{B}^T \delta \mathbf{f}_l + \delta \mathbf{B}^T \mathbf{f}_l \\ &= \mathbf{B}^T \mathbf{K}_l \mathbf{B} \delta \mathbf{p} + \mathbf{K}_{geo} \delta \mathbf{p} \end{aligned} \quad (17)$$

The result is the rotated local stiffness matrix plus the geometric stiffness matrix.

$$\mathbf{K} = \mathbf{B}^T \mathbf{K}_l \mathbf{B} + \mathbf{K}_{geo} \quad (18)$$

The derivation and details of the geometric stiffness matrix can be found in Crisfield [18]. Note that he uses a different coordinate system.

3. Gravity

This section describes how distributed loads such as gravity can be added to the co-rotational model. The method used assumes the load is distributed uniformly over the element. This can also be used for other distributed loads such as water current.

3.1. Equivalent forces and moments

The global forces at the first node are a function of the distributed force vector \mathbf{q} , which contains the distributed forces in the global coordinate system.

$$\bar{\mathbf{F}}^q = \frac{1}{2} L_0 \mathbf{q} \quad (19)$$

The global forces at the second node are equal to the global forces at the first node. The moments at the first node are first calculated in the local coordinate system. The moment around the local x-axis is zero since the external forces have no influence on torsion. The moment around the local y-axis is due to all

forces in \mathbf{e}_3 -direction. The minus sign is due to the right-hand-rule. The moment around the local z-axis is due to all forces in \mathbf{e}_2 -direction. The moments at the first node are represented by:

$$\mathbf{M}_l^q = \frac{1}{12} L_0^2 \begin{bmatrix} 0 \\ -\mathbf{q}^T \mathbf{e}_3 \\ \mathbf{q}^T \mathbf{e}_2 \end{bmatrix}. \quad (20)$$

These moments can be rotated to the global coordinate system using element triad E from (3).

$$\mathbf{M}^q = \mathbf{E} \mathbf{M}_l^q \quad (21)$$

The moments at the second node are minus the moments at the first node. Now the element force vector due to distributed forces becomes as follows:

$$\mathbf{F}^q = \begin{bmatrix} \bar{\mathbf{F}}^q \\ \mathbf{M}^q \\ \bar{\mathbf{F}}^q \\ -\mathbf{M}^q \end{bmatrix} \quad (22)$$

3.2. Consistent tangent stiffness

Since these forces are a function of the displacements, a tangent stiffness matrix needs to be derived in order to maintain quadratic convergence using the Newton-Raphson method. This matrix is derived by taking the variation of \mathbf{F}^q . The variation of the forces at each node $\bar{\mathbf{F}}^q$ is zero since $\delta \mathbf{q} = 0$. Therefore the first three rows and rows 7-9 of the stiffness matrix are zero. The variation of \mathbf{M}^q is calculated as follows.

$$\delta \mathbf{M}^q = \delta \mathbf{E} \mathbf{M}_l^q + \mathbf{E} \delta \mathbf{M}_l^q \quad (23)$$

This yields the following contribution to the stiffness matrix:

$$\mathbf{K}_q = \begin{bmatrix} 0 \\ \mathbf{K}_{sub} \\ 0 \\ -\mathbf{K}_{sub} \end{bmatrix}. \quad (24)$$

Note that 0 on the first and third row represents a 3x12 zero matrix. The matrix \mathbf{K}_q has size 12x12. \mathbf{K}_{sub} is given by the following 3x12 matrix.

$$\mathbf{K}_{sub} = \frac{1}{12} L_0^2 (-\mathbf{q}^T \mathbf{e}_3 Q(\mathbf{r}_2) + \mathbf{q}^T \mathbf{e}_2 Q(\mathbf{r}_3) - \mathbf{e}_2 \mathbf{q}^T Q(\mathbf{r}_3) + \mathbf{e}_3 \mathbf{q}^T Q(\mathbf{r}_2)) \quad (25)$$

Here $Q(\mathbf{r}_i)$ is from (11).

4. Buoyancy

The treatment of buoyancy forces is based on Yazdchi [19]. In his work the buoyancy forces are directly related to the finite element method. Yazdchi divides the distributed loads in three sections. First the forces due to distributed pressure, second the forces due to curvature of the pipe and lastly the forces due to capped ends.

4.1. Distributed pressure

The forces due to distributed pressure can be calculated as follows. On a horizontal pipe section the distributed force in N/m is

$$q_b = (A_0\rho_w - A_i\rho_i)g. \quad (26)$$

Here A_0 is the outer section area of the pipe, A_i is the inner section area of the pipe, ρ_w is the density of the sea water, ρ_i is the density of the fluid in the pipe and g is the standard acceleration due to gravity.

This equation can be found by integrating the pressure over the surface area of the pipe. The result is determined by the pressure difference in the water. However if the pipe is not horizontal, the pressure difference between top and bottom of the pipe is smaller. Therefore the factor $\mathbf{e}_n^T \mathbf{k}$ is added.

$$\bar{q}_b = q_b \mathbf{e}_n^T \mathbf{k} \quad (27)$$

Here \mathbf{k} is a unit normal in the global z-direction. \mathbf{e}_n is a unit normal defined by \mathbf{k} and \mathbf{e}_1 , which is the unit normal in the direction of the axis of the pipe. The derivation of \mathbf{e}_n can be found in [19].

If an element is only partially submerged, the forces are distributed equivalently over both nodes. This is done by introducing factors k_A and k_B . If the pipe is completely submerged, k_A and k_B are 1/2. If only the first node (node A) is submerged, the parameters k are determined from the position of the first and second node with respect to the water line. These distances h_A and h_B are positive when the node is submerged and negative when the node is above water.

$$\begin{aligned} k_A &= \bar{h} - k_B \\ k_B &= 1/2\bar{h}^2 \end{aligned} \quad (28)$$

Here \bar{h} is calculated by

$$\bar{h} = \frac{h_A}{h_A - h_B} \quad (29)$$

Up to here the buoyancy is identical to [19]. However Yazdchi neglects all equivalent moments. These are presented here.

The moments are also distributed equivalently using factors h_{AM} and h_{BM} . If the element is completely submerged, these terms are equal to 1/12 and $-1/12$ respectively. In order to find the size of the factors when the element is partly submerged, the following steps are taken.

If only the first node is submerged, the moment at the first node can be calculated using

$$M_A = \int_0^a q \frac{\partial w}{\partial \theta_1} dx. \quad (30)$$

Here a is the distance between the first node and the water surface. The local displacement w within the element is determined by a cubic Hermite interpolation function.

By solving this integral factor k_{AM} is found. The same can be done for the moment at the second node to find k_{BM} .

$$\begin{aligned} k_{AM} &= \frac{1}{4}\bar{h}^4 - \frac{2}{3}\bar{h}^3 + \frac{1}{2}\bar{h}^2 \\ k_{BM} &= \frac{1}{4}\bar{h}^4 - \frac{1}{3}\bar{h}^3 \end{aligned} \quad (31)$$

The equivalent nodal forces can now be found.

$$\mathbf{F}_1^b = \bar{q}_b \begin{bmatrix} k_A L \mathbf{e}_n \\ k_{AM} L^2 (\mathbf{e}_1 \times \mathbf{e}_n) \\ k_B L \mathbf{e}_n \\ k_{BM} L^2 (\mathbf{e}_1 \times \mathbf{e}_n) \end{bmatrix} \quad (32)$$

Here \mathbf{e}_n is the direction of the equivalent forces and $(\mathbf{e}_1 \times \mathbf{e}_n)$ is the direction of the equivalent moments.

4.2. Curvature effects

The forces due to curvature effects are also implemented as given by Yazdchi. Note that he uses a different coordinate system.

$$\mathbf{F}_2^b = q_b \begin{bmatrix} h_A \tan \theta_1 \mathbf{e}_3 - h_A \tan \phi_1 \mathbf{e}_2 \\ \mathbf{0} \\ -h_B \tan \theta_2 \mathbf{e}_3 + h_B \tan \phi_2 \mathbf{e}_2 \\ \mathbf{0} \end{bmatrix} \quad (33)$$

The third row is the negative of the first row because of the direction of rotation at the second node. Note that the force \mathbf{F}_2^b is dependent on the water depth. The force is only applied on submerged nodes.

4.3. Capped ends

Thirdly Yazdchi also gives a buoyancy term due to capped ends. This term is applied to an end of the pipe.

$$\mathbf{F}_2^b = q_b \begin{bmatrix} h_A \mathbf{e}_1 \\ \mathbf{0} \\ -h_B \mathbf{e}_1 \\ \mathbf{0} \end{bmatrix} \quad (34)$$

5. Hydrodynamic forces

Hydrodynamic forces are calculated using Morison's equation [20]. The following equation is Morison's equation for a moving pipe in moving water.

$$\mathbf{q}_{Morison} = \frac{1}{2} \rho C_d D \dot{\mathbf{d}}_{rn} |\dot{\mathbf{d}}_{rn}| + \rho C_a \frac{\pi}{4} D^2 \ddot{\mathbf{d}}_{rn} + \rho \frac{\pi}{4} D^2 \ddot{\mathbf{d}}_{wn} \quad (35)$$

Here ρ is the density of the water, C_d is the drag coefficient, D is the pipe diameter, $\dot{\mathbf{d}}_{rn}$ and $\ddot{\mathbf{d}}_{rn}$ are the relative velocity and relative acceleration in normal direction of the pipe. C_a is the added mass coefficient.

The first term of (35) is the drag force, the second term is the added mass force. The last term is due to the pressure gradient, called the Froude-Krylov force. This force is a function of the acceleration of the water in normal direction $\ddot{\mathbf{d}}_{wn}$.

The relative velocity is calculated from the difference between the water velocity and the pipe velocity. The same can be done for the relative acceleration.

$$\begin{aligned} \dot{\mathbf{d}}_r &= \dot{\mathbf{d}}_w - \dot{\mathbf{d}} \\ \ddot{\mathbf{d}}_r &= \ddot{\mathbf{d}}_w - \ddot{\mathbf{d}} \end{aligned} \quad (36)$$

The relative velocity in the normal direction of the pipe is calculated by subtracting the tangential relative velocity from the relative velocity. Again the same can be done for the relative normal acceleration.

$$\begin{aligned}\dot{\mathbf{d}}_{rn} &= \dot{\mathbf{d}}_r - \dot{\mathbf{d}}_r^T \mathbf{e}_1 \mathbf{e}_1 \\ \ddot{\mathbf{d}}_{rn} &= \ddot{\mathbf{d}}_r - \ddot{\mathbf{d}}_r^T \mathbf{e}_1 \mathbf{e}_1\end{aligned}\quad (37)$$

The velocities and acceleration of the pipe are determined by the HHT- α time integration method. The velocities and acceleration of the water are determined by the Airy wave theory.

6. Results

The numerical model formed from the equations described in this paper is implemented in C++ using the FeaTure framework for finite element codes [25]. This section shows static and dynamic results from several examples.

6.1. Static: Buoyancy

To validate the buoyancy forces, the reaction forces of three examples are compared to analytical results. The analytic results are obtained using Archimedes Law.

$$F = A_o \rho_w g L \quad (38)$$

Here $A_o L$ is the volume of the pipe and ρ_w is the density of the water.

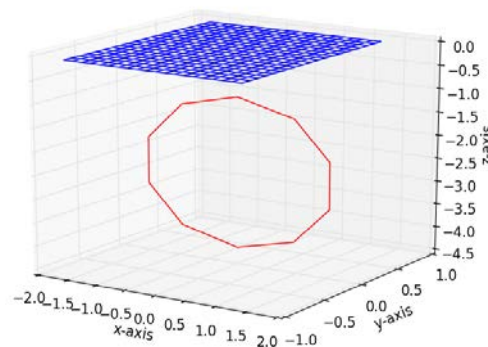


Figure 2. Pipe inclined at $x = 0$ and deformed to a circle using prescribed deformations

Table 1. Buoyancy forces [N]

Example	Analytical	Numerical
Vertical	315.89	315.89
Horizontal	157.95	157.95
Circle	3158.9	3158.9

In the three buoyancy examples the outer diameter is set to $d = 0.2$ m. The density of the water is set to $\rho_w = 1025$ kg/m³. The first example is a vertical pipe of length $L = 1$ m inclined at the water surface. Numerically the buoyancy force is determined by the capped end term. The second example is a horizontal pipe of length $L = 1$ m supported at both ends. The third example is a pipe inclined at $x = 0$ and deformed to a circle using prescribed deformations. This example is depicted in Figure 2. The blue area is the water surface area.

In Table 1 the analytical and numerical solutions of the three examples are given. It can be seen that the numerical solutions are equal to the analytical solutions.

In the example with the horizontal pipe, the pipe is slightly curved due to the buoyancy forces. Thus curvature forces are acting on the pipe. The curvature forces are a function of the water depth. Thus if the pipe is moved downward, the curvature forces become larger and the total buoyancy force becomes smaller.

6.2. Static: Convergence

In the next example a pipe with a diameter of 457 mm and wall thickness 31 mm is considered. Other properties can be found in Table 2. This pipe placed 10 m above water. A distributed load of -3000 N/m is applied to the beam in the first two steps. In the third step the buoyancy forces are added. The result is shown in Figure 3. The blue area in this figure is the water surface.

Table 2. Beam properties

Parameter	Size
Length	100 m
E-modulus	207 GPA
Poisson ration	0.3
Density pipe	7700 kg/m ³
Density water	1025 kg/m ³

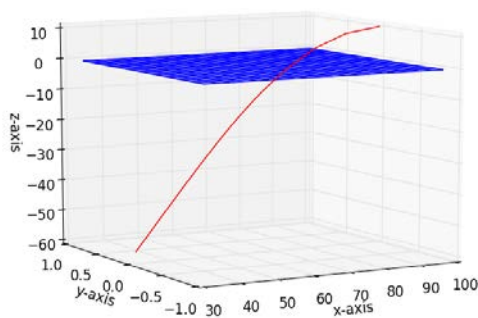


Figure 3. Deformed pipe resulting from three load steps; two steps of distributed load and one step of buoyancy

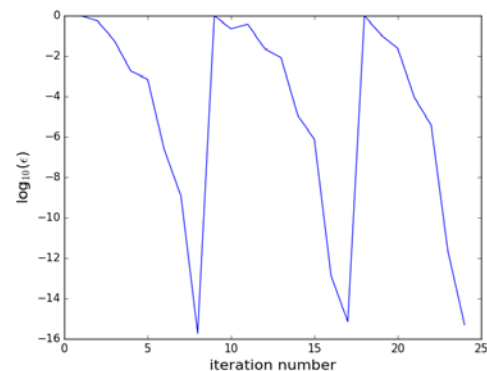


Figure 4. Convergence using displacement based error

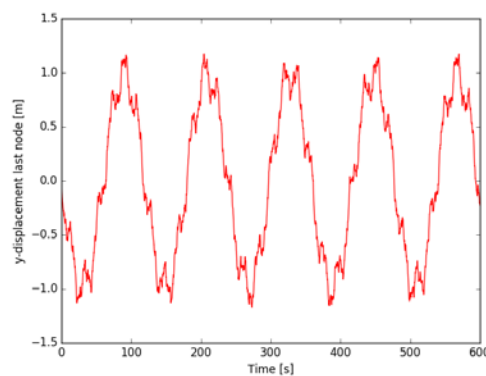
The convergence using the tangential stiffness matrix is depicted in Figure 4. As expected for the Newton-Raphson iteration method, this convergence is quadratic. Furthermore the convergence is checked using a numerical stiffness matrix instead of the tangential stiffness matrix. No difference in convergence was observed.

6.3. Dynamic: Small deformations by force

In this example a cantilever beam subject to small deformations is considered. The length of this beam is $L = 100$ m and it is divided in 10 elements. Width and height of the beam are 0.1 m. Only in the first time step a load of $F = 1000$ N is applied at the free end of the beam. This example is solved using the HHT- α method with $\alpha = 0$. This is equal to the Newmark- β method with parameters $\alpha = 1/2$ and $\beta = 1/4$. The results of the y-displacement of the end of the beam is shown in Figure 5.

Table 3. Eigenfrequencies [Hz] of the cantilever beam

n	Analytical	Numerical
1	0.00838	0.00834
2	0.0525	0.0525
3	0.147	0.147
4	0.288	0.288
5	0.476	0.473
6	0.711	0.703

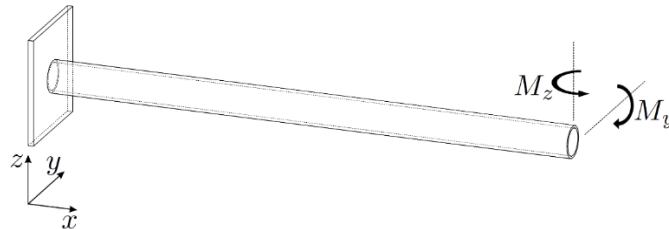
**Figure 5.** Response of beam tip to impulse load

In Table 3 the eigenfrequencies of the result shown in Figure 5 are compared to the analytically calculated eigenfrequencies of a cantilever beam. It is observed that these eigenfrequencies correspond very well to the numerical results.

6.4. Dynamic: Numerical damping

In this section the effect of the numerical damping in the HHT- α method is checked using an example problem. In this problem a cantilever beam is loaded with two equally large moments at the tip. The first moment is around the y-axis, the second moment is around the z-axis. This is depicted in Figure 6

The diameter of the pipe is 559 mm (22 inch) and the wall thickness is 21 mm. The beam is divided into 10 elements. Other pipe properties are given in Table 2. Using a time step of $\Delta t = 0.1$ s the displacements are calculated until total time of 60 s is reached.

**Figure 6.** Example problem numerical damping

Two cases are considered. The first case is without numerical damping, thus $\alpha = 0$. The second case is with $\alpha = 0.03$. The total displacement of the tip of the pipe is calculated. The Fourier transform of the total displacement is depicted in Figure 7 and Figure 8. In these figures it can be observed that the HHT- α method shows numerical dissipation for the 3rd eigenfrequency, around 1 Hz, and higher. The calculation time and required number of iterations to converge is depicted in Table 4.

The HHT- α method is not unconditionally stable for nonlinear systems. This is observed by increasing the time period calculated. When using no numerical damping the system becomes unstable after approximately 300s. This problem is solved by including the numerical damping by setting $\alpha = 0.03$.

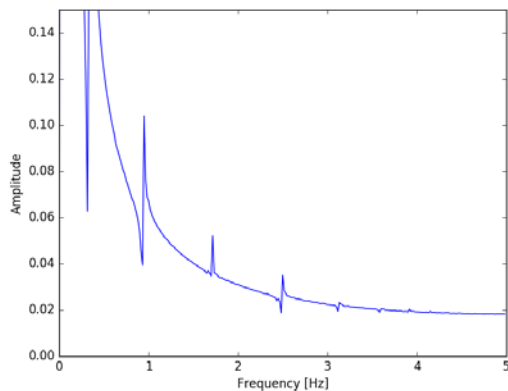


Figure 7. Fourier transform of example without numerical damping

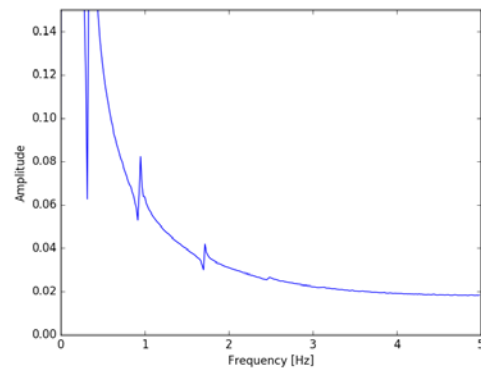


Figure 8. Fourier transform of example including numerical damping

Table 4. Number of iterations and calculation time of HHT method

α	Iterations per step	Calculation time
0	3-4	2.3 s
0.03	2-3	1.7 s

6.5. Dynamic: Hydrodynamic forces

A massless pipe with a length of 100 meters is placed horizontally 100 meter below the water surface. The pipe has a diameter of 0.2 m and a wall thickness of 50 mm. The mesh consists of 10 elements and the water density is 1025 kg/m³. At time $t = 0$ the pipe is horizontal and the displacements are zero. Figure 9 shows the result of the dynamic calculation without Morison forces. Figure 10 shows the results including Morison forces. It can be seen that the displacements u and w in x - and z -direction damp out quickly.

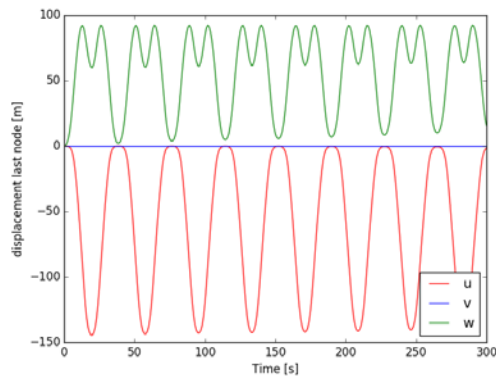


Figure 9. Displacement of the tip of a massless pipe under buoyancy load without Morison forces

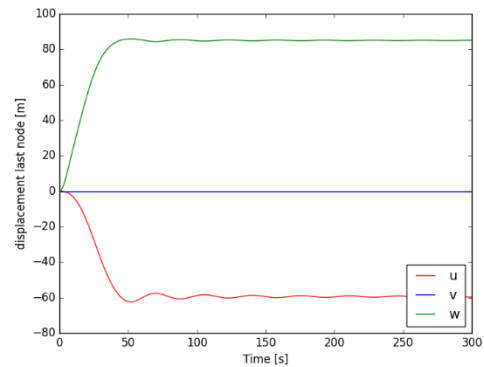


Figure 10. Displacement of the tip of a massless pipe under buoyancy load including Morison forces

6.6. Dynamic: Pipe response to vessel movement

A pipe with diameter of 457 mm (18 inch) with a wall thickness of 31 mm is considered. The pipe has a length of 200m. A section of length 100 m is supported by the pipe laying vessel. The centre of motion of the vessel is placed at the middle of the supported section. The unsupported part of the pipe is divided in 10 elements. Other pipe properties can be found in Table 2.

A distributed load of -3000 N/m is exerted on the pipe in vertical direction. When the pipe is below the water surface at $z = 0$ buoyancy forces act on the pipe. The static solution of this example can be found in Figure 11.

The movement of the centre of motion of the vessel is a response to the wave by Response Amplitude Operators (RAO) [26][27]. The wave motion is determined by a Pierson-Moskowitz spectrum [28] based on significant wave height H_s and mean zero crossing up period T_z [29]. This spectrum represents a fully developed sea. Figure 12 shows the response of the vessel's centre of motion to an irregular wave with significant wave height $H_s = 3$ m and mean zero crossing up period $T_z = 7$ s. Figure 13 shows the displacement of the free end of the pipe with respect to the static solution.

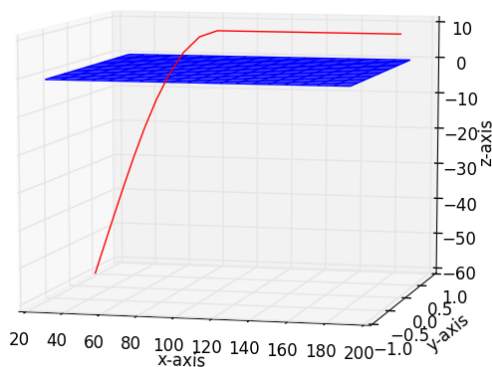


Figure 11. Static solution of pipe partly supported by vessel

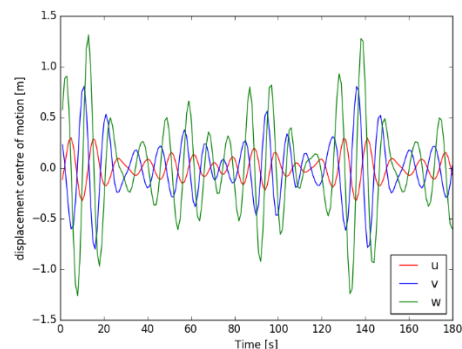


Figure 12. Displacement of vessel's centre of motion

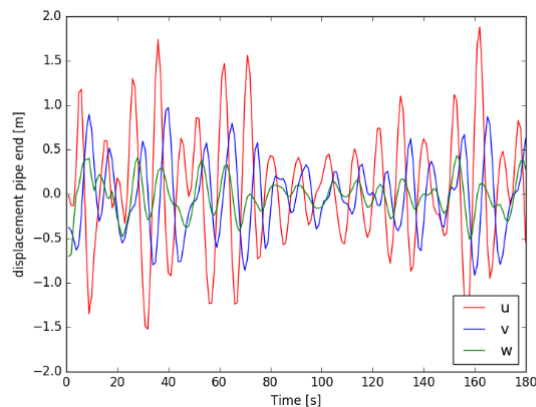


Figure 13. Displacement with respect to static solution of free pipe end

7. Conclusion

The nonlinear co-rotational finite element model presented in this paper shows good results for buoyancy forces and gravity forces. Furthermore, the static convergence is quadratic due to the Newton-Raphson method in combination with a consistent tangent stiffness matrix, resulting in an efficient calculation.

The implicit HHT- α method used for numerical time integration works well with buoyancy load and gravity. Numerical damping prevents instability problems. Furthermore, the Morison forces result in damping in the system.

References

- [1] Malahy R C 1985 A nonlinear finite element method for the analysis of the offshore pipe laying problem (Rice University)
- [2] Wood Group *PipeLay* <https://www.woodgroup.com/> [Accessed: 16-Aug-2017].
- [3] Orcina Ltd *OrcaFlex* <https://www.orcina.com/SoftwareProducts/OrcaFlex/> [Accessed: 16-Aug-2017]
- [4] Reissner E 1972 On one-dimensional finite-strain beam theory: the plane problem *J. Appl. Math. Physic* **23(5)**
- [5] Simo J C 1985 A finite strain beam formulation. The three-dimensional dynamic problem. Part I *Comput. Methods Appl. Mech. Eng.*, **49(1)**, pp. 55–70
- [6] Simo J C and Quoc L V 1986 A three-dimensional finite-strain rod model. Part II: computational aspects *Comput. Methods Appl. Mech. Eng.* **58(1)** pp. 79–115
- [7] Shabana A A, Hussien H A and Escalona J L 1998 Application of the Absolute Nodal Coordinate Formulation to Large Rotation and Large Deformation Problems *J. Mech. Des.* **120(2)**
- [8] Newmark N M 1959 A method of computation for structural dynamics *J. Eng. Mech. Div.* **85(3)** pp. 67–94
- [9] Romero I 2008 A comparison of finite elements for nonlinear beams: the absolute nodal coordinate and geometrically exact formulations *Multibody Syst. Dyn.* **20** pp. 51–68
- [10] Bauchau O A, Han S, Mikkola A and Matikainen M K 2014 Comparison of the absolute nodal coordinate and geometrically exact formulations for beams *Multibody Syst. Dyn.* **32(1)** pp. 67–85
- [11] Shabana A A 1983 A coordinate reduction technique for dynamic analysis of spatial substructures with large angular rotations *J. Struct. Mech.* **11(3)** pp. 401–31
- [12] Disveld H J 2017 *Simulation of nonlinear pipeline dynamics development of a recursive method* MSc thesis: University of Twente CTW.16/TM-5788

- [13] Crisfield M A 1990 A consistent co-rotational formulation for non-linear, three-dimensional, beam-elements *Comput. Methods Appl. Mech. Eng.*, **81(2)** pp. 131–50
- [14] Nour-Omid B and Rankin C C 1991 Finite rotation analysis and consistent linearization using projectors *Comput. Methods Appl. Mech. Eng.* **93(3)** pp. 353–84
- [15] Le T 2013 *Nonlinear Dynamics of Flexible Structures Using Corotational Beam Elements* (KTH Royal Institute of Technology)
- [16] Li Z X 2007 A co-rotational formulation for 3D beam element using vectorial rotational variables *Comput. Mech.* **39(3)** pp. 309–22
- [17] Crisfield M A 1991 *Non-linear Finite Element Analysis of Solids and Structures: Volume 1* (John Wiley & Sons)
- [18] Crisfield M A 1997 *Nonlinear Finite Element Analysis of Solids and Structures, Volume 2* (John Wiley & Sons)
- [19] Yazdchi M and Crisfield M A 2002 Non-linear dynamic behaviour of flexible marine pipes and risers *Int. J. Numer. Methods Eng.* **54(9)** pp. 1265–308
- [20] Morison J, Johnson J and Schaaf S 1950 The force exerted by surface waves on piles *J. Pet. Technol.* **2(5)**
- [21] Hilber H M, Hughes T J R and Taylor R L 1977 Improved numerical dissipation for time integration algorithms in structural dynamics *Earthq. Eng. Struct. Dyn.* **5(3)** pp. 283–92
- [22] Rodrigues O 1840 Des lois géométriques qui régissent les déplacements d'un système solide dans l'espace: et de la variation des coordonnées provenant de ces déplacements considérés indépendamment des causes qui peuvent les produire *J. Math. Pures Appl.* **5** pp. 380–440,
- [23] Spurrier R A 1978 Comment on 'Singularity-free extraction of a quaternion from a direction-cosine matrix *J. Spacecr. Rockets* **15(4)** p. 255
- [24] Cook R D, Malkus D S, Plesha M E and Witt R J 2002 *Concepts and applications of finite element analysis, 4th Ed.* (John Wiley & Sons)
- [25] van den Boogaard A H 2006 *FeaTure: A finite element analysis toolkit for use in a research environment* [Online]. Available: www.utwente.nl/en/et/ms3/research-chairs/nsm/-facilities/software/feature_/. [Accessed: 16-Aug-2017].
- [26] Dean R G and Dalrymple R A 1991 *Water wave mechanics for engineers and scientists (Vol. 2)*. (World Scientific Publishing Co Inc.)
- [27] Faltinsen O M 1993 *Sea loads on ships and offshore structures* (Cambridge University Press.)
- [28] Pierson W J and Moskowitz L 1964 A proposed spectral form for fully developed wind seas based on the similarity theory of SA Kitaigorodskii *J. Geophys. Res.* **69(24)**
- [29] Barltrop N D P and Adams A J 1991 *Dynamics of fixed marine structures, 3th ed.* (Butterworth-Heinemann)